Backscattering of Neutrons and Emergence of Secondary Gamma Rays from Iron Slabs Bombarded by 15-MeV Neutrons

AUTHOR(S):

BAN, Shuichi; SHIN, Kazuo; HYODO, Tomonori

CITATION:

BAN, Shuichi ...[et al]. Backscattering of Neutrons and Emergence of Secondary Gamma Rays from Iron Slabs Bombarded by 15-MeV Neutrons. Memoirs of the Faculty of Engineering, Kyoto University 1979, 41(2): 137-147

ISSUE DATE:

1979-06-30

URL:

http://hdl.handle.net/2433/281098

Backscattering of Neutrons and Emergence of Secondary Gamma Rays from Iron Slabs Bombarded by 15-MeV Neutrons

By

Shuichi BAN, Kazuo SHIN and Tomonori HYODO

(Received December 25, 1978)

Abstract

Backscattered neutrons and associated gamma rays from iron slabs for 15-MeV incident neutrons were measured by a 2″ϕ×2″ NE-213 scintillator. The associated particle method was used to confine the neutron beam. The time-of-flight method was used auxiliarily to eliminate thermal neutron capture gamma rays, and to estimate the time-independent neutron background. Experimental spectra were compared with the results of the Monte Carlo calculations. Values of the neutron albedo and the secondary gamma ray albedo were shown as functions of slab thickness. These values showed good agreement with the Monte Carlo calculations.

1. Introduction

Backscattering of neutrons and emergence of secondary gamma rays associated with the incidence of D-T neutrons to materials are very important for the design study of the blanket and ducts of fusion reactors and collimators of radiation therapies.

The neutron albedo has been measured for fission neutrons and thermal neutrons incident on materials in slab geometry[1)~3)]. During et al.[4)] measured the spectra of back scattered neutrons from iron and aluminum slabs with respect to incident 15-MeV neutrons. The energy angle distributions of neutrons, however, were not published in their paper.

Calculation of neutron albedos for iron were performed by Allen et al.[5)] for 14 MeV neutrons by the Monte Carlo method. Their results were given as differential with respect either to the energy or to the direction, but not to both.

For the purpose of estimating the dose rate of secondary gamma rays emerging from the surface of materials accompanied by the irradiation of neutrons, the secondary

Department of Nuclear Engineering

gamma-ray albedo is used frequently as the ratio of the dose rate of emerging secondary gamma rays to incident neutrons[6]. Coleman et al.[3] calculated the secondary gamma-ray albedo by the Monte Carlo method for neutrons in energy up to 200 KeV.

In the present work, neutron and secondary gamma-ray differential albedos were measured for iron slabs. The neutron source was D-T neutrons and the detector was a liquid organic scintillator NE-213. For the purpose of comparing experimental data, a Monte Carlo calculation was carried out. A Monte Carlo code was composed for the neutron transport with a highly anisotropic scattering. A discrete ordinate S_n code ANISN[7] and a gamma-ray transport Monte Carlo code were used for the secondary gamma rays, and integral estimations were made for gamma-ray production cross sections.

Experimental

Deuterium ions, accelerated by a 200-keV Cockcroft-Walton type accelerator, were incident to a tritiated zirconium target, and produced D-T neutrons. The associated particle method[8], i.e. the coincident counting of neutrons and alpha particles emerging from the ^{3}H(d, n)^{4}He reaction, was used to produce a well collimated neutron beam. The polar angle of the coincidence cone was 2.3°. The average neutron energy was 14.9 MeV, considereing the emitting angle.

A schematic drawing of the experimental setup is shown in Fig. 1. An iron slab was placed at 200 cm from the target and perpendicular to the axis of the coincidence cone. A detector was placed at 60cm from the point of crossing of the axis to the surface of the slab. It detected the backscattered neutrons and secondary gamma rays emerging from the slab at 120° of the polar angle.

The energy spectra of neutrons and gamma rays were obtained for the slab thickness of 5, 10 and 15 cm. The width and height of the slabs were 60 and 80 cm, respectively. A lead and heavy concrete shadow shieled of 120 cm in thickness was placed between the detector and the neutron source.

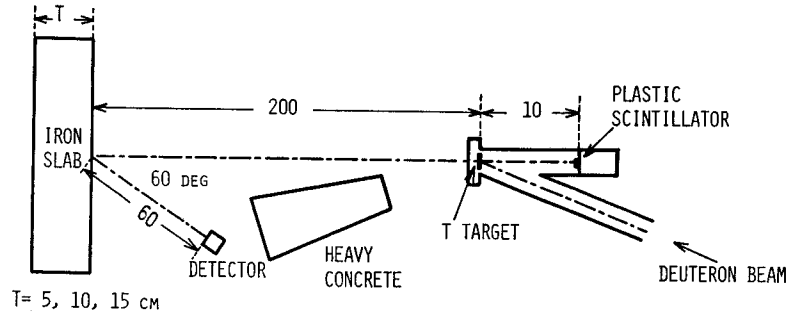

Fig. 1. Schematic drawing of experimental setup.

The block diagram of electronic circuits used in this experiment is shown in Fig. 2. The alpha particle emerging from the target was detected with a thin plastic scintillator, which was placed at an angle of 150° with respect to the deuteron beam. The thickness of the scintillator was so thin that it was not sensible for neutrons, gamma rays or beta particles emerging from the target. The coincidence cone of the neutrons was decided by the angle to be subtended by this plastic scintillator.

The coincidence time resolution for 15-MeV neutrons was 1.5 ns at FWHM. A coincidence gate, the width being approximately 40 ns was applied to decrease random coincidence and to eliminate thermal neutron capture gamma rays. The time-of-flight method was not applied for the measurement of neutron spectra because of poor resolution for neutrons above 10 MeV. The method was, however, used for the measurements of the background caused by ransom coincidence.

The output pulses from the photomultiplier tube were amplified and stored in a two-dimensional pulse-height analyzer with the aid of a rise-time-to-pulse-height converter[9]. The number of pulses accumulated in each bit of neutron and gamma-ray zone were summed up in each energy channel of the neutrons and gamma rays, respecti-

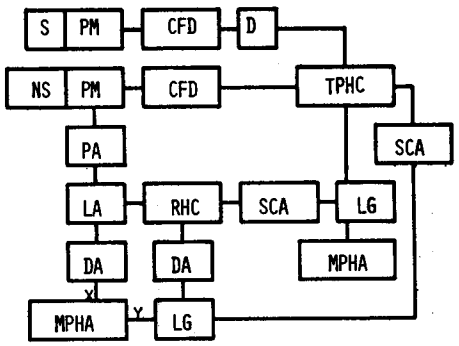

S: Plastic Scintillator
NS: Liquid Scintillator; NE-213
PM: Photomultiplier Tube; RCA 8575
CFD: Constant Fraction Discriminater
D: Delay
TPHC: Time to Pulse Height Converter
PA: Preamplifier
LA: Linear Amplifier
DA: Delay Amplifier
RHC: Risetime to Pulse Height Converter
SCA: Single Channel Analyzer
LG: Linear gate
MPHA: Multichannel Pulse Height Analyzer

Fig. 2. Block diagram of the electronic system used.

vely, and the pulse height distributions for neutrons and gamma rays were obtained. The unfolding of the pulse-height distributions to energy spectra was done by the FERDO code[10] for gamma rays and by the SAND II code[11] for neutrons. The initial neutron spectra for SAND II code were obtained by the differential method.

A random coincidence of output pulses of two detectors caused by unrelated events was the source of the time-independent background. A measurement was done without the iron slab to determine the pulse height distribution of the background. The background was subtracted from each pulse height distribution with the slab. This background was normalized by the use of neutron flight time distributions before flight time zero. The time dependent background was negligibly small when the shadow bar was placed between the detector and the scatterer.

The neutrons' slowing down time in the iron slab was calculated by the Monte Carlo method. It was less than 10 ns for neutrons between 2 to 15 MeV. The slowing down time to thermal neutrons was longer than the gate time width, because neutrons must be slowed down by elastic scattering for their energy less than 860 keV (1st exitation level of iron). The pulses from the NE-213 scintillator caused by the thermal neutron capture gamma rays were discriminated by the coincidence gate.

The gamma-ray yield in the NE-213 scintillator caused by the 14.9 MeV neutron irradiation was measured, and the unfolded spectrum is shown in Fig. 3. The main component of gamma rays is 4.43-MeV inelastic gamma rays from the first excitation

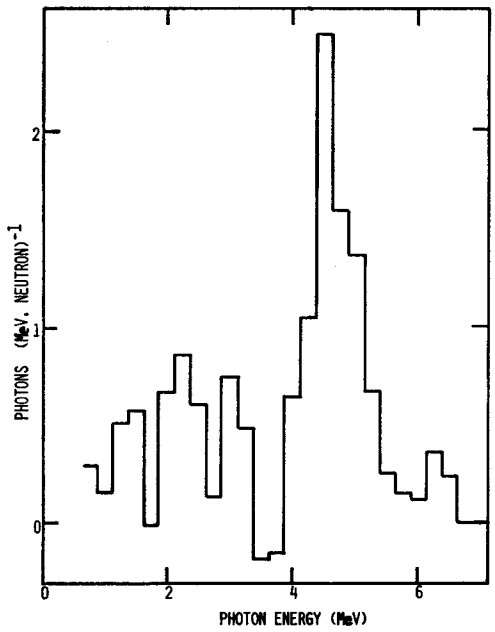

Fig. 3. Gamma-rays caused by 15 MeV neutrons incident to NE-213 scintillator.

level of ^{12}C in the scintillator. The gamma-ray flux of this energy may be less than 1 percent of the flux of incident neutrons.

Calculations

Neutron Albedo Calculation

Monte Carlo calculations were carried out to obtain the value of a fast neutron albedo. Scattering of 15-MeV neutrons has characteristics of a very strong anisotropy.

Elastic scattering angles were sampled, using the Coveyou technique[12] which is used in the O5R code. Inelastic scattering angles were sampled isotropically, and the weights were determined using differential cross sections. Flux distortion appeared for discrete angles because of using the discrete angle method (Coveyou technique). Singly sacttered neutrons are the dominant component in fast neutron albedos, so this distortion appears strongly. The expected value was used for the reduction of variance. The following probability was added after each collision,

$$P=WF(\Omega)\ d\Omega\frac{e^{-\Sigma_T r}}{r^2}$$

F: the probability that a neutron is scattered toward the measuring point,
r: distance between the scattering point and the measuring point,
Σ_T: total macroscopic cross section,
W: weight before the collision.

$F(\Omega)$ was calculated from the differential cross section directly.

Differential cross sections of elastic and inelastic scatterings were represented using the Legendre polinomials (P_{20} in maximum).

$$\frac{d\sigma}{d\Omega}=\frac{\sigma}{2\pi}\sum_{l=0}^{n}\frac{2l+1}{2}f_l P_l(\mu)\quad n\leq 20 \tag{1}$$

or they were represented using a partial-range linearly anisotropic representation. The cross-sections were taken from the ENDE/B-IV library. The differential cross sections were well represented by formula (1) and negative fluxes did not appear for any reactions between 2 to 15 MeV.

The energy cutoff was 2 MeV in this calculation, and the weight cutoff was not used.

Secondary Gamma Ray Albedo Calculation

Calculation of the production of gamma rays from the iron slab was performed by the coupling of the calculation of neutron flux distribution and the Monte Carlo calculation of gamma ray yield. Neutron flux distributions within the materials were calculated, using the S_N code ANISN[7] in the S_{15}-P_8 approximation. DLC-2D[13] 100 group neutron data taken from the END/B-III library were used.

The secondary gamma-ray sources in each spacial mesh were as follows.

$$S(E_G)=\int M_{NON}(E)\ \Sigma_{NON}(E)\ \phi(E)\ P(E_G,E)\ dE \tag{2}$$

where,

E_G: gamma ray energy
E: neutron energy
ϕ: calculated neutron flux
Σ_{NON}: non elastic cross section
M_{NON}: gamma-ray multiplicity for all non-elastic events
P: secondary gamma-ray energy distribution.

It was assumed that neutron fluxes were distributed within the coincidence cone. The data of M_{NON}, Σ_{NON} and P were taken from ENDF/B-IV. The contribution of neutrons below 2.26 MeV to the gamma-ray yield was less than 1%, so the calculations were performed only for neutrons above 2.26 MeV. It was assumed that gamma-ray productions were isotropic in the laboratory system.

In succession to the calculations of the secondary gamma-ray distributions, gamma-ray transport calculations were performed by the Monte Carlo code[14]. Another calculation was performed by ANISN using DLC-28.

Results and Discussion

Measured and calculated spectra at the detector were normalized to the fluxes per MeV per cm^2 per incident neutron. The spectra obtained by the ANISN code were normalized correcting the solid angle.

Neutron Albedos

Measured and calculated energy spectra are shown in Fig. 4 for a slab of 5 cm in thickness. They show fair agreement in both spectra. A broad peak at 12–15 MeV is attributed to elastic and inelastic scattering from lowlying discrete levels. The increase of neutrons at 2–5 MeV results from the process of (n, 2n) reaction and inelastic scattering from the continuum. This process is relatively dominant for the backward angle because these neutrons are emerging isotropically.

The calculated spectrum is approximately 30% larger than the measured values at 8–10 MeV. The measured values are not accurate in this region because of an unfolding error.

Spectra for a slab of 10 cm in thickness are shown in Fig. 5. In comparison with the slab of 5 cm in thickness, they show very similar forms with the spectra in Fig. 4, and approximately 20% larger as a whole. The spectra for a slab of 15 cm in thickness

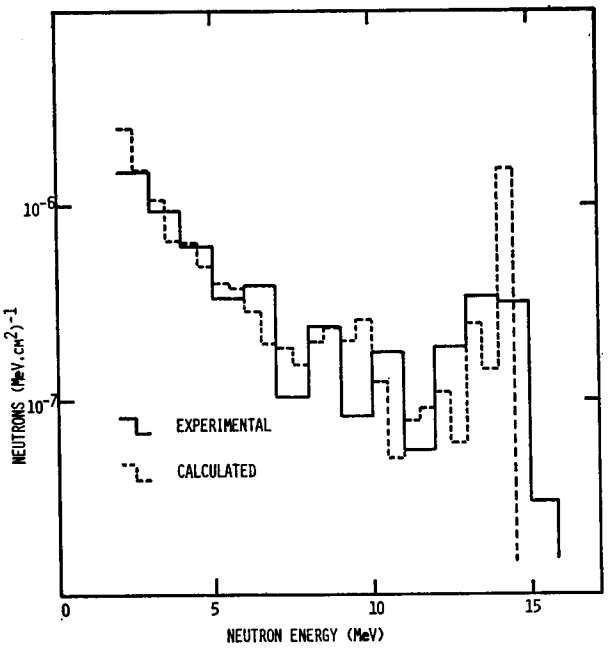

Fig. 4. Backscattered neutron spectrum at 120° for a slab of 5 cm in thickness.

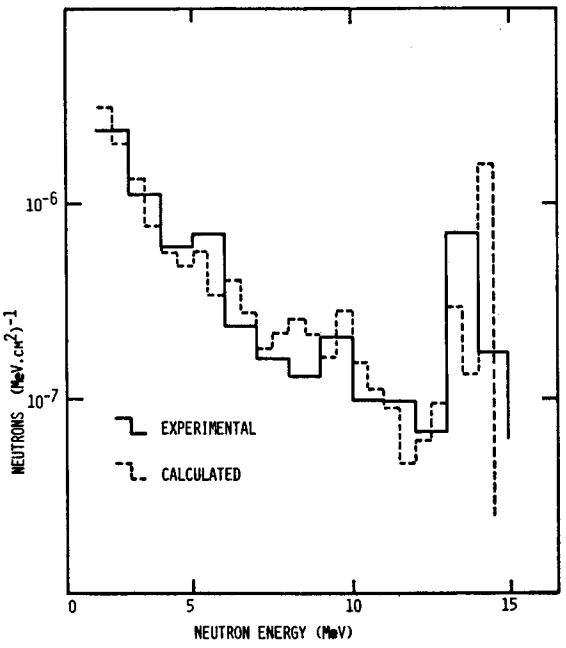

Fig. 5. Backscattered neutron spectrum at 120° for a slab of 10 cm in thickness.

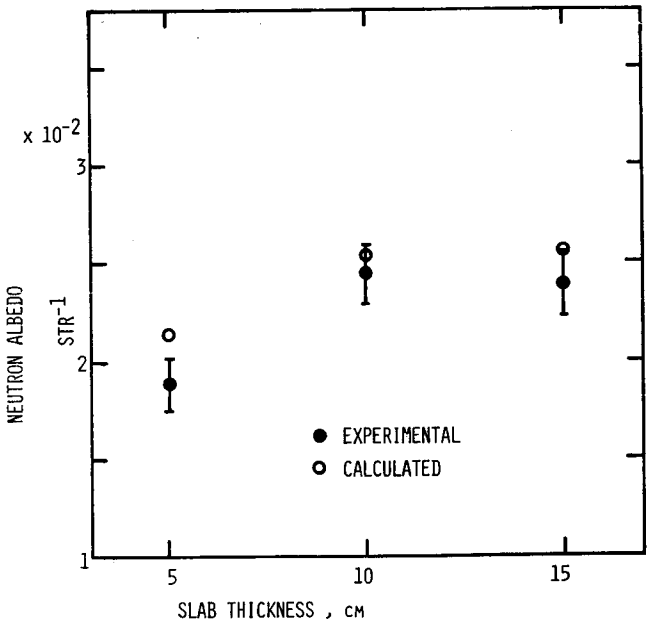

Fig. 6. Differential number albedo of neutron at 120° for 2–15 MeV region.

were almost the same as those for the 10-cm thick slab, and they are not shown in this paper.

Values of the differential number albedos at 120° and for the 2–15 MeV neutrons are shown in Fig. 6 as functions of slab thickness. The values of measured albedos are approximately 5% smaller than the calculated values. The major cause of this discrepancy may be the background counts of the plastic scintillator used to detect alpha particles in the coincidence cone.

Secondary Gamma-ray Albedos

Measured and calculated spectra for slabs of 5 cm and 10 cm in thickness are shown in Fig. 7 and 8, respectively. The calculated spectra have no clear peaks, and the measured spectra oscillate in the high energy region. This oscillation may be caused by a statistical error amplified by unfolding for a minority of incident gamma photons to the detector.

These data were arranged as a form of secondary gamma-ray dose albedos, such as the ratio of dose rate of secondary gamma rays to that of incident neutrons, and shown in Fig. 9 as a function of slab thickness. These values saturate more rapidly than the values of neutron albedos with an increase of slab thickness. The calculated albedo values are less than the experimental values. Calculated values by the ANISN code were in good agreement with the Monte Carlo calculations.

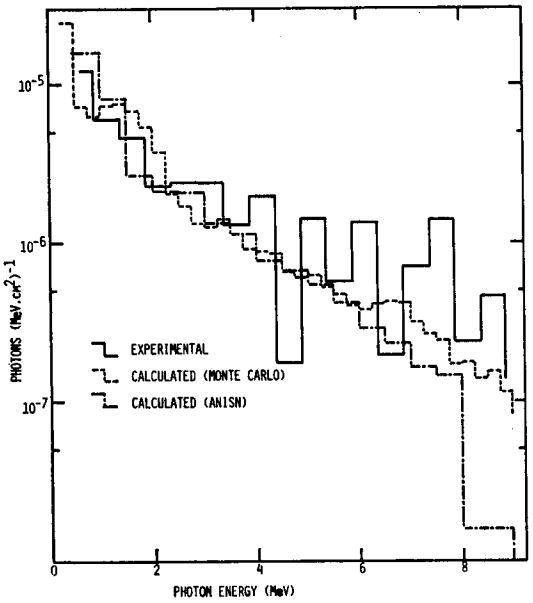

Fig. 7. Secondary gamma-ray spectrum at 120° for a slab of 5 cm in thickness. Solid line: Experimental results. Dashed line: Calculated results by Monte Carlo method. Dash-dotted line: Calculated results by ANISN.

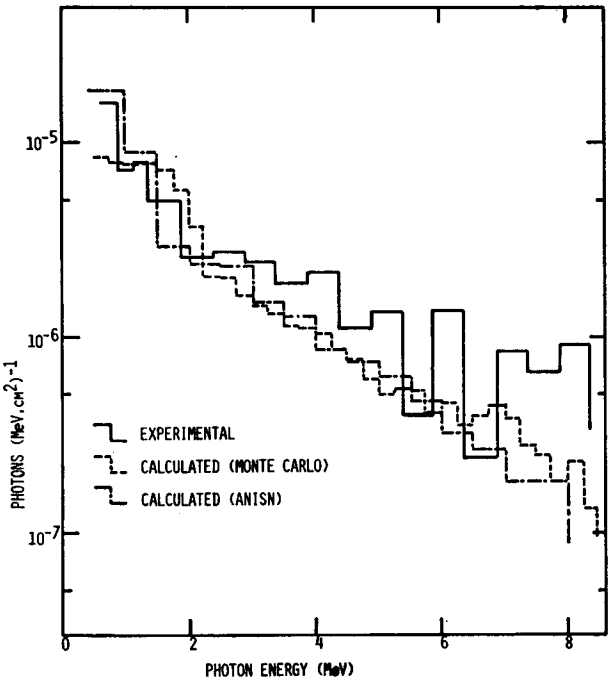

Fig. 8. Secondary gamma-ray spectrum at 120° for a slab of 10 cm in thickness.

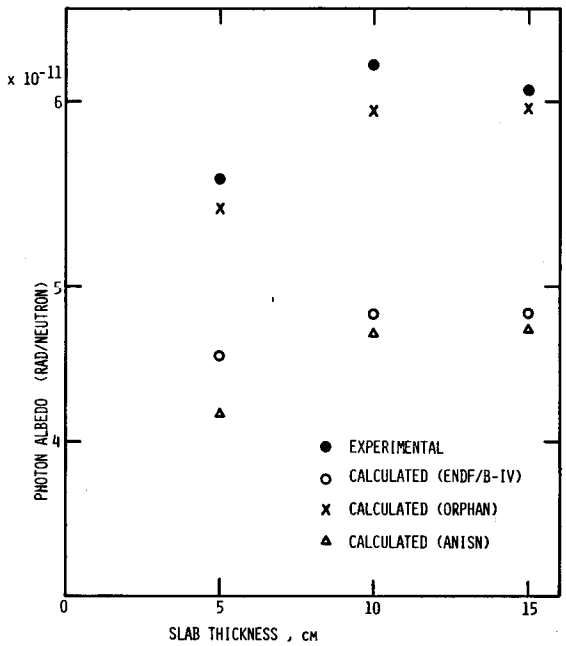

Fig. 9. Secondary gamma-ray dose albedos at 120° for 0.62–9 MeV region. They are normalized for one incident neutron and at point 1 cm from incident point. Three calculated results are shown: 1) by Monte Carlo method using ENDF/B-IV data, 2) by Monte Carlo method using Orphan's data, 3) by ANISN using group cross section DLC-28.

Two experimental data of neutron induced gamma-ray production cross sections by Dickens[15] and Orphan[16] were estimated in ENDF/B-IV. They are approximatedy 40% different from each other for neutrons at 11–15 MeV region. The data by Dickens[15], after the correction of errors in the normalization of the previous data set, agreed well with the results of Orphan. The gamma-ray multiplicity obtained by Orphan[16] was used for neutrons of 13–15 MeV. The calculated values using this data were in good agreement with the experimental results as shown in Fig. 9.

Conclusion

Backscattered neutrons and associated gamma rays from iron slabs for 15-MeV indicent neutrons were measured by the organic scintillator NE-213. The associated particle method was used to confine the neutron beam. The time-of-flight method was used auxiliarily to eliminate thermal neutron capture gamma rays and to estimate the time-independent neutron background. Experimental spectra are shown in comparison with the results of the Monte Carlo calculations. Experimental spectra have oscillation enlarged by unfolding because of a small number of pulses. Values of the neutron

albedos and the secondary gamma ray albedos are shown as functions of slab thickness. These values show good agreement with the Monte Carlo calculations.

Acknowledgement

The authors want to express their thanks to Messrs. H. Fujita and T. Kanazawa for their contribution of a set up of the experiment, and to Messrs. Y. Motoishi and T. Hasegawa for their sasistance with the experiment.

References

1) R. E. Maerker and F. J. Muckenthaler; Nucl. Sci. Eng., **22**, 455 (1965).
2) R. E. Maerker and F. J. Muckenthaler; Nucl. Sci. Eng., **26**, 339 (1966).
3) W. A. Coleman et al.; Nucl. Sci. Eng., **27**, 411 (1967).
4) During et al.; Arkiv für Physik, **26**, No. 19, 293 (1963).
5) F. J. Allen et al.; BRL-1199, Ballistic Research Laboratories (1963).
6) W. E. Selph; ORNL-RSIC-21, Oak Ridge National Laboratory (1968).
7) W. W. Engle, Jr.; K-1693, Union Carbide Corp. (1967).
8) G. C. Bonazolla et al.; Nucl. Instr. Methods, **87**, 291 (1970).
9) S. Kinbara et al.; Nucl. Instr. Methods, **70**, 137 (1969).
10) W. R. Burrus and V. V. Verbinski; AND-SD-2, 148, American Nuclear Society (1964).
11) S. Berg and W. N. McElroy; AFWL-TR-67-41, Vol. II, Air Force Weapons Laboratory (1967).
12) R. R. Coveyou et al.; ORNL-3622, Oak Ridge National Laboratory (1965).
13) R. Q. Wright; ORNL-TM-3049, Oak Ridge National Laboratory (1969).
14) Y. Hayashida, private communication.
15) J. K. Dickens et al., Nucl. Sci. Eng., **62**, 515 (1977).
16) V. J. Orphan et al.; Nucl. Sci. Eng., **57**, 309 (1975).